AIAA JOURNAL
Vol. 48, No. 4, April 2010

Elastic Properties of Open-Cell Foams with Tetrakaidecahedral Cells Using Finite Element Analysis

Prasanna Thiyagasundaram,* Bhavani V. Sankar,† and Nagaraj K. Arakere‡
University of Florida, Gainesville, Florida 32611-6250

DOI: 10.2514/1.J050022

A finite-element-method-based micromechanics has been used for predicting the orthotropic properties of open-cell foams that have tetrakaidecahedral unit cells. Foams with equisided and Kelvin-elongated tetrakaidecahedron as unit cells are studied. The results for elastic constants from the finite element models agree well with those of available analytical models. The struts were modeled using both Euler–Bernoulli and Timoshenko beam elements. It is found that classical beam theory overpredicts the elastic moduli when the struts have smaller length-to-thickness ratios. The effect of varying strut cross section on the elastic constants is studied. The variation is assumed to be such that the strut cross section gradually decreases from maximum value at the support ends to minimum value at the beam midsection. It is found that for the same relative density, foams with varying cross sections have much lower elastic moduli than foams with uniform cross sections.

Nomenclature

A	=	cross-sectional area of the strut
a_1	=	length of the representative volume element
a_2	=	width of the representative volume element
a_3	=	height of the representative volume element
b	=	dimension of the top and the bottom squares of the elongated tetrakaidecahedron unit cell
$[C]$	=	stiffness matrix of the foam
d	=	length of the side of the equilateral triangle cross section
f_{ij}	=	force in direction i when displacement is applied in direction j
I_x, I_y	=	moment of inertia in the X and the Y directions
E_i	=	Young's modulus along axis i
E_s	=	elastic modulus of the strut material
G_{ij}	=	shear modulus in direction j on the plane for which the normal is in direction i
J	=	torsion constant
L	=	dimension of the long edges of the elongated tetrakaidecahedron unit cell
l	=	length of each individual edge (strut) of the equisided tetrakaidecahedron
r	=	radius of the three-cusp hypocycloid cross section
V	=	volume of the representative volume element
u_i	=	displacement in the i direction
Δu_i	=	difference in translational displacement along axis i
$\Delta\theta_i$	=	difference in rotational displacement along axis i
ε_{ij}	=	macrostrain
ε_0	=	applied macrostrain
ε_1, ε_2, ε_3	=	strain components in the principal X, Y, and Z directions
ν_{ij}	=	Poisson's ratio
ν_s	=	Poisson's ratio of the strut material
ρ_s	=	density of the strut material
ρ/ρ_s	=	relative density of the foam

Received 22 June 2009; revision received 11 October 2009; accepted for publication 22 October 2009.

*Graduate Student, Department of Mechanical Engineering, P.O. Box 116250; pthiyaga@ufl.edu (Corresponding Author).

†Newton C. Ebaugh Professor, Department of Mechanical Engineering; sankar@ufl.edu. Associate Fellow AIAA.

‡Associate Professor, Department of Mechanical and Aerospace Engineering; nagaraj@ufl.edu.

I. Introduction

CELLULAR solids are materials made out of solid strut or thin platelike structures bridged together. They occur in nature in the form of honeycombs, wood, bone, cork, etc. These materials possess a unique combination of properties such as low thermal conductivity, low density, and high energy absorption [1]. Foams are a class of cellular solids, generally made by dispersing gas into a liquid material and then cooling it to solidify. They are categorized as open-cell and closed-cell foams. Depending on the solid materials that are made into foams, they are also categorized as polymeric foams, metallic foams, and ceramic foams [1]. Because of developments in materials science and manufacturing techniques, advanced foams have found potential for use in automobile, aircraft, and space vehicle structures. A special example is the use of foams in external fuel tanks and thermal protection systems of space vehicles. It has been accepted that packed in a body-centered cubic structure, a tetrakaidecahedron (a 14-faced polyhedron) satisfies the minimum surface energy condition for monodispersed bubbles [2]. Microcellular graphitic carbon foams were first developed at the U.S. Air Force Research Laboratory in the 1990s [3]. Clearly, it has been proven that the repeating unit cell of this foam can be approximated by a regular tetrakaidecahedron [4].

The catastrophic failure of Space Shuttle *Columbia* in February 2003 has given the necessary impetus to understand and reduce the likelihood and severity of foam-shedding events that occur from the shuttle's external fuel tanks. Currently, there is ongoing research focused on understanding the mechanisms that cause foam fracture and debris liberation [5]. This mandates a thorough understanding of the foam's mechanical response behavior, and characterization of its elastic properties is the first step in that direction.

In the same context, there is also ongoing research in the field of aerostructural composites focused on characterizing materials using principles of micromechanics [6,7]. These methods are based on simulating a characteristic representative part of the structure that periodically repeats itself, instead of simulating the entire model. Foams with simple representative unit-cell structures from cube [8] to hexagonal cell structures to a regular tetrakaidecahedron [4,9] as the unit cell have been carefully studied and have been characterized for their mechanical behavior.

Currently, BX-265 and NCFI24-124 are the two foams used most exclusively in space shuttle external tanks. The photomicrographs [10] of these two foams are shown in Figs. 1a and 1b. Analysis of the foam structure from these micrographs has shown that due to forming

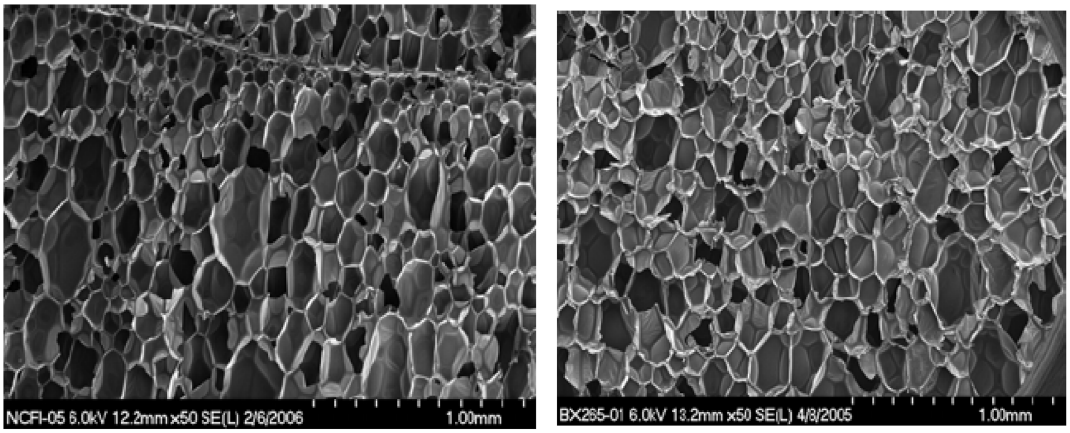

a) NCFI24-124 **b) BX-265**

Fig. 1 Photomicrographs of foams used in insulation of external fuel tanks of space vehicles a) NCFI24-124 and b) BX-265 [10].

and rising processes that take place during fabrication, the unit cell of these foams is elongated in one of the three principal directions. Hence, this unit cell is called an elongated tetrakaidecahedron and the elongated direction is referred to as the rise direction. This makes the elongated foam strictly orthotropic.

Broadly, the available literature on foam mechanics can be classified into characterizing foams based on experimental studies [10–12] or characterizing foams based on analytical models [13,14].

Analytical models that have been developed focus primarily on predicting the mechanical and strength properties. Assuming that the unit-cell edges behave like a three-dimensional beam, the mechanics of deformation of the tetrakaidecahedron unit cell leads to a set of equations for the effective Young's modulus, Poisson's ratio, and tensile strength of the foam in the principal material directions [10]. The equations for these elastic constants have been derived and written in terms of the cell edge length and the axial, flexural, and torsional rigidities of the strut cross section. The variation of these properties with relative density (the ratio of the density of the cellular medium to the density of the solid strut material) of the foam has also been expressed.

The current paper explores the possibility of using finite-element-based micromechanics procedures to calculate the elastic properties of foam materials. To do this, periodic boundary conditions have been derived and applied to the unit-cell model. The results obtained from this method have been compared with the results obtained from existing analytical models [10] and they have been shown to match well for some of the elastic constants. The advantages of using finite-element-based methods over analytical methods have also been highlighted.

The analytical model by Zhu et al. [14] for predicting the elastic moduli, Poisson ratios, and shear moduli has been used for comparison with the foam modeled with equisided tetrakaidecahedron as a unit cell. The analytical model by Sullivan et al. [13] has been used for comparison with the foam modeled with elongated tetrakaidecahedron as the unit cell. The requisite expressions from both these papers [13,14] are reproduced in the Appendix, for completeness.

II. Finite Element Modeling of a Tetrakaidecahedron Unit Cell

In general, a tetrakaidecahedron has 24 vertices and 36 edges comprising eight six-sided polygons and six four-sided polygons (Fig. 2). It is more precisely called a truncated octahedron, since it is created by truncating the corners of an octahedron [15]. A regular tetrakaidecahedron is generated by truncating the corners of a cube [14]. This is called an equisided tetrakaidecahedron. If it is generated by truncating the corners of a cuboid or hexahedron, it is called an elongated tetrakaidecahedron [10]. An equisided tetrakaidecahedron has all edges of equal length.

In this study, the commercially available ABAQUS® finite element software is employed for developing the model. A model for the equisided tetrakaidecahedron is shown in Fig. 2. The principal directions X, Y, and Z are considered to be along the lines passing through the centers of the squares (Fig. 2) on the front and back, the left and right, and the top and the bottom, respectively. Including the squares and the hexagons, the tetrakaidecahedron unit cell is made up of 24 beam elements.

The geometry and the material properties of the constituent strut material used in the equisided tetrakaidecahedron model are listed in Table 1. The strut material is considered as isotropic. In the current example, the beam cross sections are approximated to be an equilateral triangle. The dimensions required to completely describe an equisided tetrakaidecahedron unit cell are shown in Fig. 3: namely, the length of the strut of the unit cell (L) and the side of the equilateral triangle (d). The beam cross sections are oriented such that the bisector of one of the angles of the triangular cross section at the center of the strut passes through the unit-cell center (Fig. 4). The cross-sectional properties used in the model are also listed in Table 1.

Similar to an equisided tetrakaidecahedron, the geometry and the material properties of the constituent strut material used in the elongated tetrakaidecahedron model are listed in Table 2. The strut material is again considered to be isotropic. Actual microstructural measurements [10] indicate that the strut cross section in polyurethane foams is actually a three-cusp hypocycloid (Fig. 5).

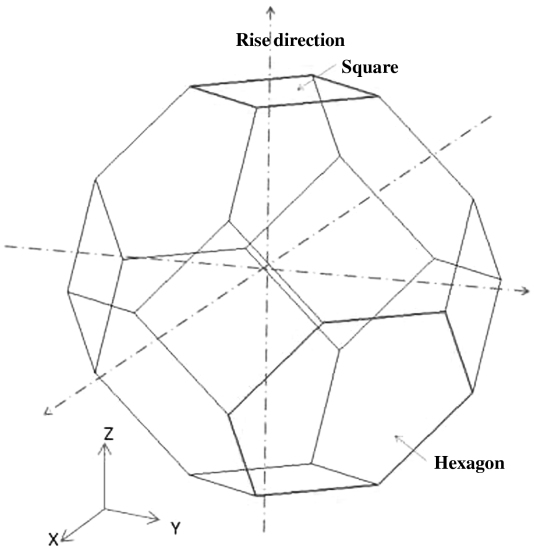

Fig. 2 Equisided tetrakaidecahedron geometry: eight hexagons and six squares.

Table 1 Material properties of the strut, geometric properties, and cross-sectional properties of the equisided tetrakaidecahedron unit cell

Material properties of the strut	
Density, ρ_s, kg/m^3	1650
Elastic modulus, E_s, GPa	23.42
Poisson ratio, ν_s	0.33
Geometry of the equisided tetrakaidecahedron unit cell (Fig. 3)	
L, mm	1
d, mm	0.06
Relative density	0.001653
Cross-sectional properties (equilateral triangle)	
Cross-sectional area, A, m^2	1.5588×10^{-9}
Moment of inertia, I_x, I_y, m^4	2.3382×10^{-19}
Torsion constant, J, m^4	4.6765×10^{-19}

The dimensions required to completely describe the elongated tetrakaidecahedron unit cell are shown in Fig. 5: namely, the length of the strut of the unit cell on the top and the bottom squares (b), the length of all the other struts (L), the radius of the three-cusp hypocycloid cross section (r), and the orientation of the struts (θ). The cross-sectional properties used in the model are listed in Table 2. It should be noted that even though there are 36 edges in the geometry of the tetrakaidecahedron, only 24 beam elements have been modeled. This is due to periodicity of the unit cell. Out of the six squares (three pairs: top and bottom pair, left and right pair, and front and back pair) only the top, front, and right squares are modeled, as shown in Fig. 6.

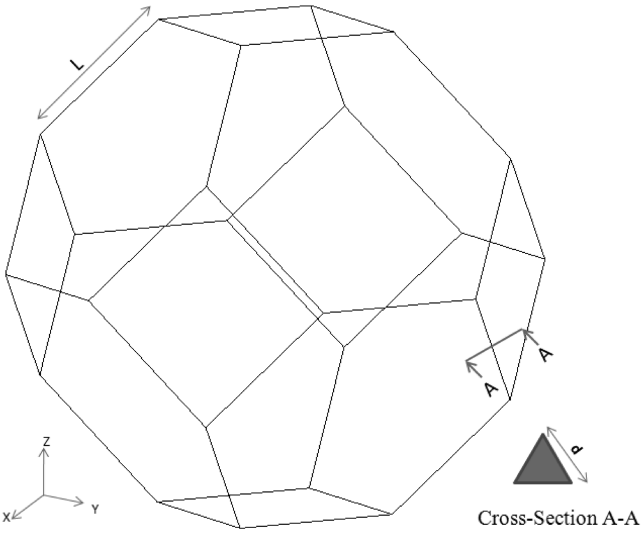

Fig. 3 Defining the geometry of an equisided tetrakaidecahedron unit cell.

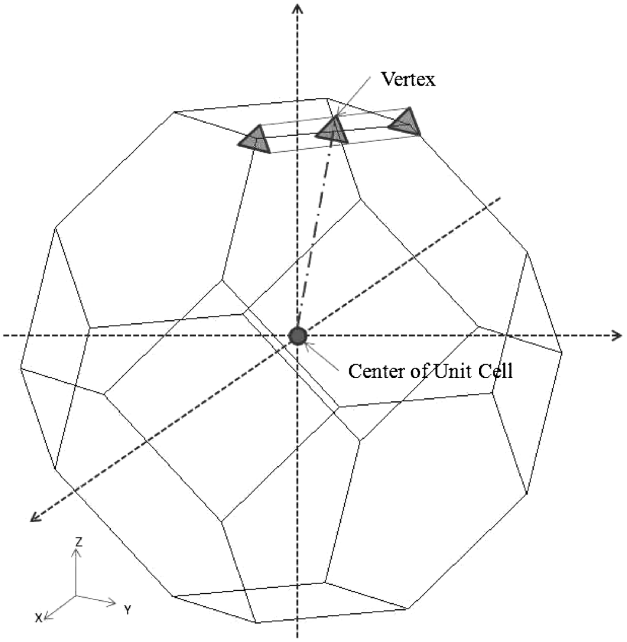

Fig. 4 Defining the orientation of the beams of the unit cell.

Table 2 Material properties of the strut, geometric properties, and cross-sectional properties of the elongated tetrakaidecahedron unit cell

Material properties of the strut	
Density ρ_s, kg/m^3	1650
Elastic modulus E_s, GPa	17
Poisson ratio ν_s	0.33
Geometry of the elongated tetrakaidecahedron unit cell (Fig. 5)	
L, μm	77.2
b, μm	35.6
θ, deg	53.57
r, μm	26
H, μm	248.85
D, μm	142.04
Relative density	0.03481
Cross-sectional properties (three-cusp hypocycloid)	
Cross-sectional area A, m^2	1.024×10^{-10}
Moment of inertia I_x, I_y, m^4	1.403×10^{-21}
Torsion constant J, m^4	2.806×10^{-21}

The use of beam elements to model the struts needs some explanation. The beam model will be valid only if the struts are slender and behave like a beam. This requires a slenderness ratio L/r' (where L is the length of the strut and r' is the radius of gyration defined by $r'^2 = I/A$) greater than about 10. If the slenderness ratio is less than 10 but greater than 6, one can use shear-deformable beam elements and hope to obtain good results. If L/r' is less than 6, one cannot use beam elements to model the deformation of the struts. One needs to resort to solid elements.

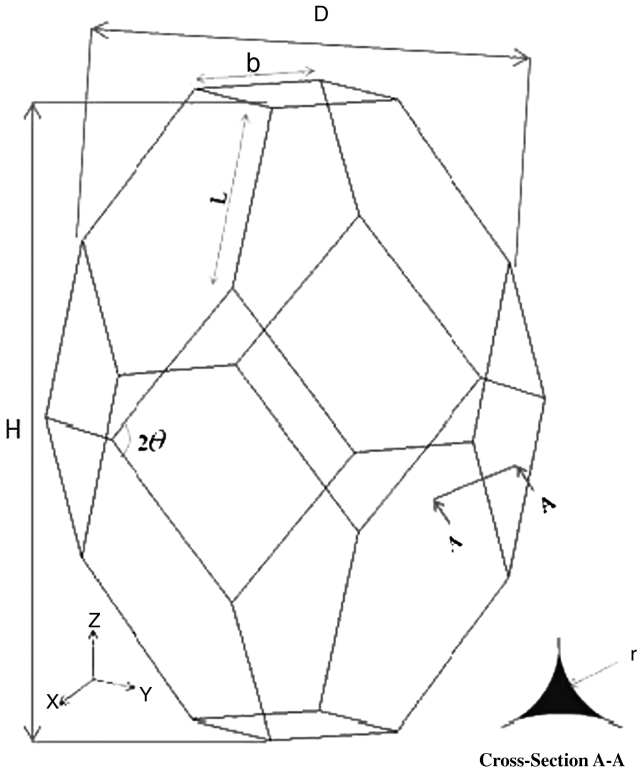

Fig. 5 Defining the geometry of an elongated tetrakaidecahedron unit cell.

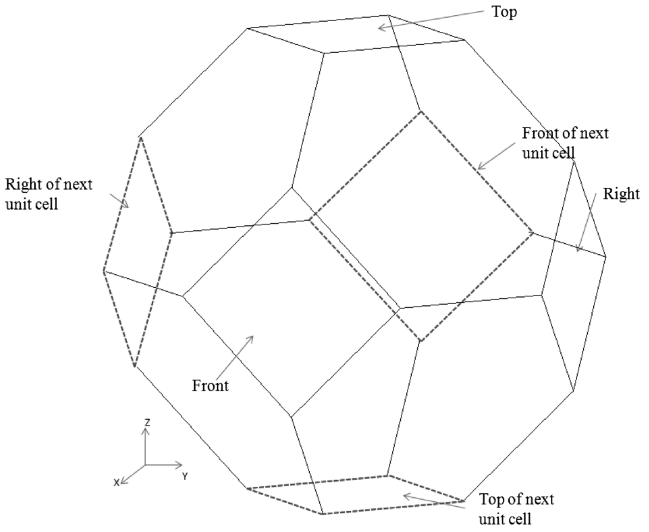

Fig. 6 Defining the geometry of an elongated tetrakaidecahedron unit cell.

For both equisided and elongated tetrakaidecahedrons, two-node beam elements (classical Euler–Bernoulli beam element, B33 in the ABAQUS material library) with cubic formulation were used to model the unit cell. Three-node quadratic elements (shear-deformable Timoshenko beam elements, B32 in the ABAQUS material library) were used in some cases to study the effects of shear deformation on the overall properties of the foam.

III. Periodic Boundary Conditions

For computing the elastic constants using micromechanics, we need equations that relate the microstrains to the corresponding macrostrains. Using these equations, the periodic boundary conditions (BCs) can be derived. From the periodicity of the cell structure (Fig. 7), the representative volume element (RVE) is identified to be the smallest cuboid that completely encloses the tetrakaidecahedron, such that six square sides of the tetrakaidecahedron are on the six faces of the cuboid.

In this section we derive the periodic boundary conditions that will be used to derive the elasticity matrix of the idealized foam. Consider the deformation gradient $\varepsilon_{ij} = u_{i,j}$. We would like to subject the RVE to a deformation such that the average of the above deformation gradient is equal to a given $\bar{\varepsilon}_{ij}$. Then this condition can be represented as

$$\bar{\varepsilon}_{ij} = \frac{1}{V}\int_V \frac{\partial u_i}{\partial x_j}\,\mathrm{d}V \tag{1}$$

where V is the RVE volume. By applying divergence theorem to the right-hand side of Eq. (1), the volume integral is converted into surface integral as

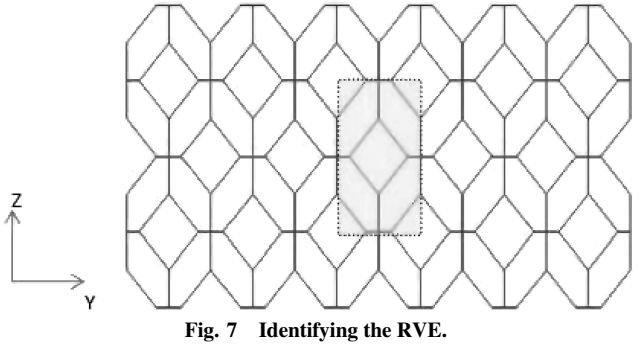

Fig. 7 Identifying the RVE.

Table 3 Periodic boundary conditions: unit normal strain $\varepsilon_{xx} = 1$[a]

Pair of node numbers	Difference in displacements U_x	U_y	U_z
Top–bottom (faces normal to the principal Z axis)			
16–2	0	0	0
14–22	0	0	0
9–6	0	0	0
11–15	0	0	0
Front–back (faces normal to the principal X axis)			
7–9	a_1	0	0
3–24	a_1	0	0
5–1	a_1	0	0
8–20	a_1	0	0
Left–right (faces normal to the principal Y axis)			
18–13	0	0	0
4–10	0	0	0
21–12	0	0	0
23–17	0	0	0

[a]The difference in rotational displacements $(\theta_x, \theta_y, \theta_z)$ between the node pairs shown is zero for all load cases.

$$\bar{\varepsilon}_{ij} = \frac{1}{V}\int_S u_i n_j\,\mathrm{d}S \tag{2}$$

where the integration is performed over the surface of the cuboid. Noting that n_j is nonzero only on two surfaces that are normal to the j direction, Eq. (2) can be written as

$$\bar{\varepsilon}_{ij} = \frac{1}{V}(u_i^{(+j)} - u_i^{(-j)})A_j \tag{3}$$

where A_j is the area of the face normal to j direction, and $u_i^{(+j)} - u_i^{(-j)}$ represents the difference in the displacements u_i on the two surfaces normal to the j direction. The superscripts $+j$ and $-j$ indicate, respectively, the two surfaces with positive and negative normals in the j direction. From the above equation, we obtain the periodic boundary condition as

$$(u_i^{(+j)} - u_i^{(-j)}) = \bar{\varepsilon}_{ij}\frac{V}{A_j} = \bar{\varepsilon}_{ij}a_j, \qquad i, j = 1, 3 \tag{4}$$

Then the periodic BC for the three normal strains can be written as

$$(u_i^{(+j)} - u_i^{(-j)}) = \bar{\varepsilon}_{ii}a_i \qquad (i = 1, 2, 3;\ \text{no summation over } i) \tag{5}$$

For the case of shear strains, the periodic BCs are not unique, as the shear strain is given by the sum of two deformation gradients:

Table 4 Periodic boundary conditions: unit normal strain $\varepsilon_{yy} = 1$[a]

Pair of node numbers	Difference in displacements U_x	U_y	U_z
Top–bottom (faces normal to the principal Z axis)			
16–2	0	0	0
14–22	0	0	0
9–6	0	0	0
11–15	0	0	0
Front–back (faces normal to the principal X axis)			
7–9	0	0	0
3–24	0	0	0
5–1	0	0	0
8–20	0	0	0
Left–right (faces normal to the principal Y axis)			
18–13	0	a_2	0
4–10	0	a_2	0
21–12	0	a_2	0
23–17	0	a_2	0

[a]The difference in rotational displacements $(\theta_x, \theta_y, \theta_z)$ between the node pairs shown is zero for all load cases.

Table 5 Periodic boundary conditions: unit normal strain $\varepsilon_{zz} = 1$[a]

	Difference in displacements		
Pair of node numbers	U_x	U_y	U_z
Top–bottom (faces normal to the principal Z axis)			
16–2	0	0	a_3
14–22	0	0	a_3
9–6	0	0	a_3
11–15	0	0	a_3
Front–back (faces normal to the principal X axis)			
7–9	0	0	0
3–24	0	0	0
5–1	0	0	0
8–20	0	0	0
Left–right (faces normal to the principal Y axis)			
18–13	0	0	0
4–10	0	0	0
21–12	0	0	0
23–17	0	0	0

[a]The difference in rotational displacements $(\theta_x, \theta_y, \theta_z)$ between the node pairs shown is zero for all load cases.

Table 6 Periodic boundary conditions: unit shear strain $\gamma_{xy} = 1$[a]

	Difference in displacements		
Pair of node numbers	U_x	U_y	U_z
Top–bottom (faces normal to the principal Z axis)			
16–2	0	0	0
14–22	0	0	0
9–6	0	0	0
11–15	0	0	0
Front–back (faces normal to the principal X axis)			
7–9	0	$a_1/2$	0
3–24	0	$a_1/2$	0
5–1	0	$a_1/2$	0
8–20	0	$a_1/2$	0
Left–right (faces normal to the principal Y axis)			
18–13	$a_2/2$	0	0
4–10	$a_2/2$	0	0
21–12	$a_2/2$	0	0
23–17	$a_2/2$	0	0

[a]The difference in rotational displacements $(\theta_x, \theta_y, \theta_z)$ between the node pairs shown is zero for all load cases.

Table 7 Periodic boundary conditions: unit shear strain $\gamma_{yz} = 1$.[a]

	Difference in displacements		
Pair of node numbers	U_x	U_y	U_z
Top–bottom (faces normal to the principal Z axis)			
16–2	0	$a_2/2$	0
14–22	0	$a_2/2$	0
9–6	0	$a_2/2$	0
11–15	0	$a_2/2$	0
Front–back (faces normal to the principal X axis)			
7–9	0	0	0
3–24	0	0	0
5–1	0	0	0
8–20	0	0	0
Left–right (faces normal to the principal Y axis)			
18–13	0	0	$a_3/2$
4–10	0	0	$a_3/2$
21–12	0	0	$a_3/2$
23–17	0	0	$a_3/2$

[a]The difference in rotational displacements $(\theta_x, \theta_y, \theta_z)$ between the node pairs shown is zero for all load cases.

Table 8 Periodic boundary conditions: unit shear strain $\gamma_{xz} = 1$[a]

	Difference in displacements		
Pair of node numbers	U_x	U_y	U_z
Top–bottom (faces normal to the principal Z axis)			
16–2	$a_1/2$	0	0
14–22	$a_1/2$	0	0
9–6	$a_1/2$	0	0
11–15	$a_1/2$	0	0
Front–back (faces normal to the principal X axis)			
7–9	0	0	$a_3/2$
3–24	0	0	$a_3/2$
5–1	0	0	$a_3/2$
8–20	0	0	$a_3/2$
Left–right (faces normal to the principal Y axis)			
18–13	0	0	0
4–10	0	0	0
21–12	0	0	0
23–17	0	0	0

[a]The difference in rotational displacements $(\theta_x, \theta_y, \theta_z)$ between the node pairs shown is zero for all load cases.

$\gamma_{ij} = u_{i,j} + u_{j,i}$. Thus, one can apply either deformation gradient alone or both together. If, for example, one applies only $u_{i,j}$, then the BCs take the form

$$(u_i^{+j} - u_i^{-j}) = \bar{\gamma}_{ij} a_j; \qquad (u_j^{+i} - u_j^{-i}) = 0 \tag{6}$$

On the other hand, if one chooses $u_{i,j} = u_{j,i} = \gamma_{ij}/2$, then two sets of BCs have to be applied as shown below:

$$(u_i^{+j} - u_i^{-j}) = \frac{\bar{\gamma}_{ij} a_j}{2}; \qquad (u_j^{+i} - u_j^{-i}) = \frac{\bar{\gamma}_{ij} a_i}{2} \tag{7}$$

The above periodic BCs are explicitly presented in Tables 3–8 in the form of difference in displacements between the set of nodes for the three unit strain load cases in the three principal directions. Figures 8–10, show the pairs of node numbers that are subjected to these periodic boundary conditions. By using the reaction forces that result after the unit normal strains are applied, the stiffness matrix for the foam can be computed. It should be noted that beam elements have rotational degrees of freedom, and we need to have periodic BCs for these degrees of freedom also. Since we do not have any curvature in the foam, the corresponding periodic BCs take the form

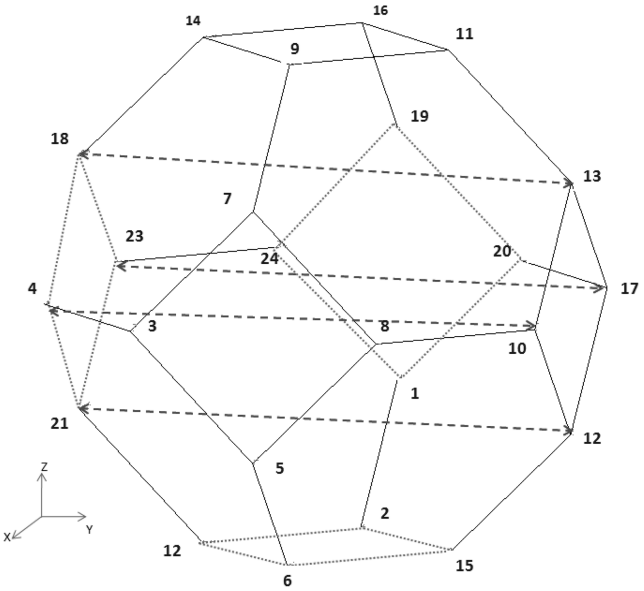

Fig. 8 Node pairs subjected to periodic boundary conditions: left and right faces.

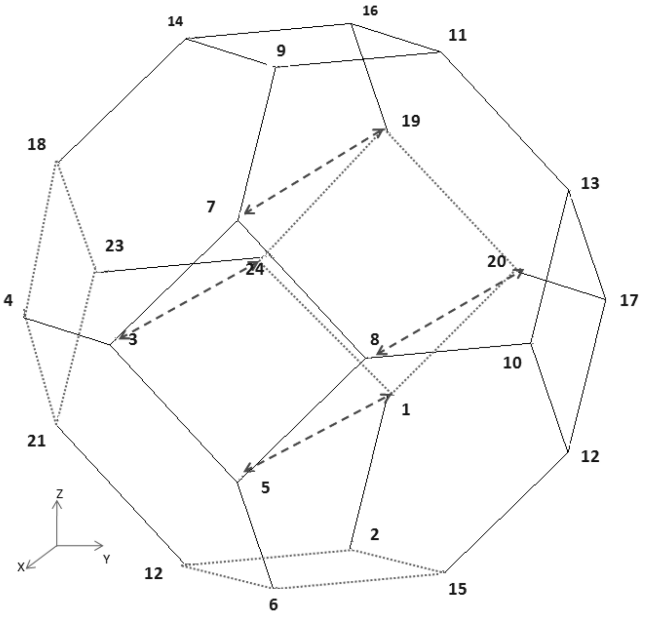

Fig. 9 Node pairs subjected to periodic boundary conditions: front and back faces.

$$(\theta_i^{(+j)} - \theta_i^{(-j)}) = 0, \qquad i, j = 1, 3 \tag{8}$$

IV. Derivation of the Elastic Constants

In this section we derive the procedures for determining the equivalent elastic constants of the tetrakaidecahedral foam idealized as an orthotropic material. The RVE of the foam is a cuboid. The equivalent orthotropic material has its principal material directions parallel to the edges of the cuboid. In this coordinate system, the normal and shear deformations are uncoupled. First, we will derive the equations to determine Young's moduli and Poisson's ratios in the principal material coordinates, 1, 2, and 3. The (macroscale) stress–strain relations of the foam are written as

$$\begin{Bmatrix} \sigma_1 \\ \sigma_2 \\ \sigma_3 \end{Bmatrix} = \begin{bmatrix} C_{11} & C_{12} & C_{13} \\ C_{21} & C_{22} & C_{23} \\ C_{31} & C_{32} & C_{33} \end{bmatrix} \begin{Bmatrix} \varepsilon_1 \\ \varepsilon_2 \\ \varepsilon_3 \end{Bmatrix} \tag{9}$$

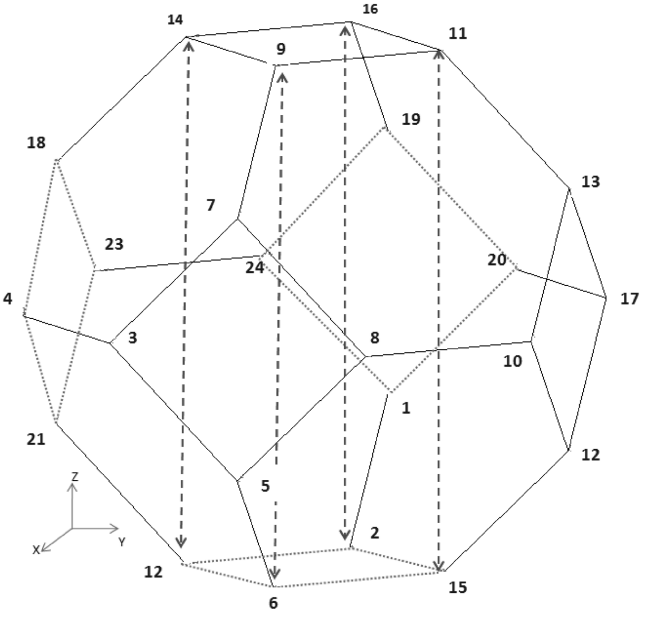

Fig. 10 Node pairs subjected to periodic boundary conditions: top and bottom faces.

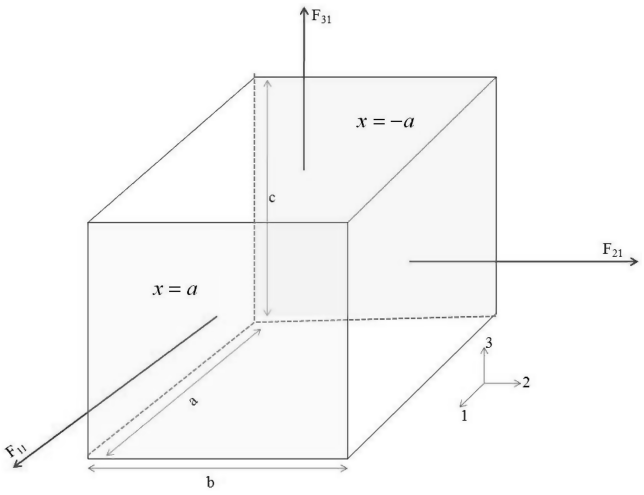

Fig. 11 RVE showing force resultants in the three directions when subjected to normal strain in the one direction on the two faces $x = a$ and $-a$.

We subject the RVE to three independent deformations such that, in each case, only one normal strain is nonzero and other two normal strains are zero. For example, in the first case we apply periodic boundary conditions such that the cuboid expands only in one direction and the strains in the other two directions are equal to zero, i.e., the dimensions of the cuboid in those directions do not change. Then the macrostrains are given by

$$\varepsilon_1 = 1, \qquad \varepsilon_2 = 0, \qquad \varepsilon_3 = 0 \tag{10}$$

Substituting Eq. (10) in Eq. (9), we get

$$\begin{Bmatrix} \sigma_1 \\ \sigma_2 \\ \sigma_3 \end{Bmatrix} = \begin{bmatrix} C_{11} & C_{12} & C_{13} \\ C_{21} & C_{22} & C_{23} \\ C_{31} & C_{32} & C_{33} \end{bmatrix} \begin{Bmatrix} 1 \\ 0 \\ 0 \end{Bmatrix} \tag{11}$$

Let the corresponding force resultants (ABAQUS output) in the three faces of the unit cell normal to the 1, 2, and 3 directions be, respectively, F_{11}, F_{21}, and F_{31} (see Fig. 11). Then the corresponding macrostresses are obtained as

$$\sigma_1 = \frac{F_{11}}{A_1}, \qquad \sigma_2 = \frac{F_{21}}{A_2}, \qquad \sigma_3 = \frac{F_{31}}{A_3} \tag{12}$$

where A_1, A_2, and A_3 are areas normal to the 1, 2, and 3 directions representing areas of the square surfaces in the 1, 2, and 3 directions of the RVE in the case of the equisided tetrakaidecahedron unit cell and representing areas of the rectangular surfaces in the 1, 2, and 3 directions of the RVE in the case of the elongated tetrakaidecahedron unit cell.

Similarly, we can deform the RVE in the other two directions and calculate second and third columns of $[C]$. These procedures are similar to those used by Karkkainen and Sankar [6].

For the case of shear, the calculations can be simplified, as there is no coupling between shear deformation and the normal deformation or between shear deformations in different planes. The periodic BCs for shear strains are given in Eqs. (6) and (7). The straightforward method of determining the shear modulus G_{ij} will be to relate the strain energy in the RVE to the strain-energy density due to shear:

$$U = \frac{1}{2} G_{ij} \gamma_{ij}^2 V \quad \text{or} \quad G_{ij} = \frac{2U}{\gamma_{ij}^2 V} \tag{13}$$

V. Effect of Varying Cross Section

It has been observed [16] that, in reality, the cross-sectional area of the struts are not uniform but they gradually vary along the length of the beam, with the cross-sectional area being maximum at the two ends of the beam and minimum at the center. For example,

Table 9 Results obtained for the properties of an equisided tetrakaidecahedron unit cell with relative density 0.1653%

Property	Finite element model			Analytical model [14]	% difference[b]
	Euler–Bernoulli (2-node cubic)	Shear-deformable (3-node quadratic)	% difference[a]		
$E_x = E_x = E_z$, GPa	46.7×10^{-6}	46.6×10^{-6}	0.24	46.4×10^{-6}	0.55
$\nu_{xy} = \nu_{yz} = \nu_{xz}$	0.498	0.498	0.11	0.497	0.14
$G_{xy} = G_{yz} = G_{xz}$, GPa	14.9×10^{-6}	14.8×10^{-6}	0.43	14.9×10^{-6}	0.35

[a]Between Euler–Bernoulli model and shear-deformable model.
[b]Between analytical model and finite element model.

Table 10 Results obtained for the properties of an elongated tetrakaidecahedron unit cell with relative density 3.45%

Property	Finite element model			Analytical model [13,17]	% difference[b]
	Euler–Bernoulli (2-node cubic)	Shear-deformable (3-node quadratic)	% difference[a]		
$E_x = E_y$, MPa	7.09	6.5	−9.04	7.07	0.29
E_z, MPa	20.63	19.28	−6.99	20.8	−0.82
$\nu_{xy} = \nu_{yx}$	0.0588	0.0757	22.28	0.0598	−1.84
$\nu_{xz} = \nu_{yz}$	0.3745	0.3694	−1.39	0.373	0.47
$\nu_{zx} = \nu_{zy}$	1.0934	1.0991	0.52	1.09	−0.31
G_{xy}, MPa	2.07	1.95	−6.03	2.06	0.39
$G_{yz} = G_{xz}$, MPa	6.74	6.25	−7.88	6.66	1.17

[a]Between Euler–Bernoulli model and shear-deformable model.
[b]Between analytical model and finite element model.

microstructural measurements [16] indicate that the cross-sectional area varies according to the following function:

$$A(x) = A_0 f(x) = A_0\left(86\frac{x^4}{l^4} + \frac{x^2}{l^2} + 1\right) \tag{14}$$

where A_0 is the Area at the midspan of the strut, x is any point along the length of the strut ($-\frac{l}{2} \le x \le +\frac{l}{2}$), and l is the length of the strut.

The elastic constants of the foam with varying cross section could be determined by following the procedures similar to that of uniform-cross-section foam. In fact, the struts can be modeled using one beam element as before but with equivalent cross-sectional properties. Since the deformations (strains, curvatures etc.) in a beam are inversely proportional to A, the equivalent uniform cross-sectional properties I and J can be readily expressed as

$$\frac{1}{A_{\text{eff}}} = \frac{1}{l}\int_{-l/2}^{l/2}\frac{\mathrm{d}x}{A(x)}, \qquad \frac{1}{I_{\text{eff}}} = \frac{1}{l}\int_{-l/2}^{l/2}\frac{\mathrm{d}x}{I(x)}$$
$$\frac{1}{J_{\text{eff}}} = \frac{1}{l}\int_{-l/2}^{l/2}\frac{\mathrm{d}x}{J(x)} \tag{15}$$

where the suffix eff denotes effective properties. To determine the above effective properties, one has to assume the nature of the cross section. In this study we assume that the cross section of the strut is an equilateral triangle. Accordingly, the cross-sectional dimension at midspan d_0, corresponding area A_0, and moments of inertia I_0 and J_0 are calculated as follows:

$$A_0 = \frac{\sqrt{3}}{4}d_0^2 \tag{16}$$

$$I_0 = \frac{\sqrt{3}}{96}d_0^4 \tag{17}$$

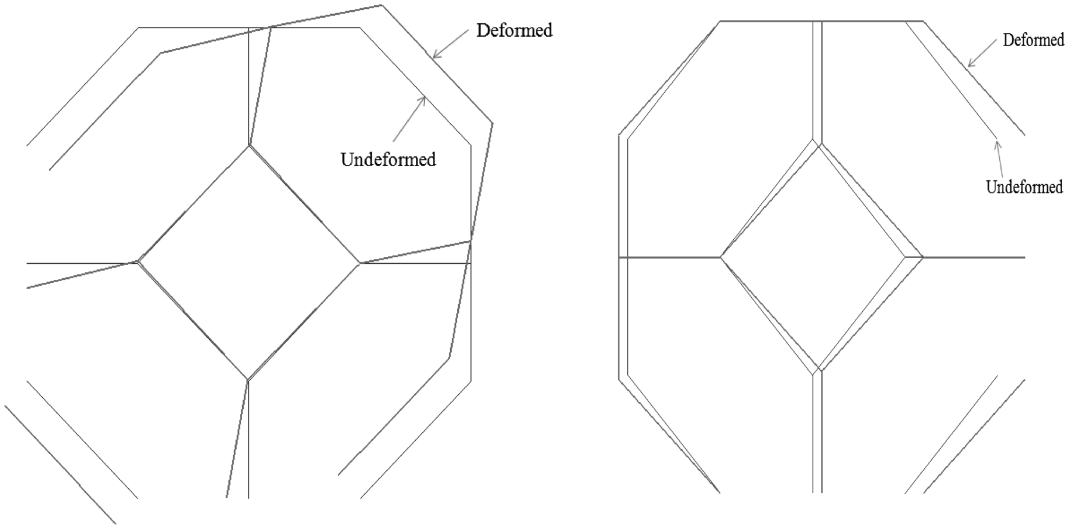

a) b)

Fig. 12 Deformed and undeformed configurations of the unit cell subjected to a) shear strain and b) normal strain.

$$J_0 = \frac{A_0^2}{5\sqrt{3}} \tag{18}$$

The variation of moments of inertia, using Eq. (14), along the length of the strut can then be written as

$$I(x) = I_0\left[86\frac{x^4}{l^4} + \frac{x^2}{l^2} + 1\right]^2, \qquad J(x) = J_0\left[86\frac{x^4}{l^4} + \frac{x^2}{l^2} + 1\right]^2 \tag{19}$$

where

$$-\frac{l}{2} \le x \le +\frac{l}{2}$$

It is desirable to compare the properties of foam with struts having a varying cross section to foam with struts having a uniform cross section. One approach to get a good comparison is by keeping the relative density the same in both cases. This can be achieved by keeping the volume of the strut the same in both cases:

$$\int_{-l/2}^{+l/2} A(x)\,\mathrm{d}x = \bar{A}l \tag{20}$$

where $\bar{A}$ is the area of the uniform cross section, and l is the length of the strut. Once $\bar{A}$ is calculated, one can determine the corresponding cross-sectional dimension $\bar{d}$ and the moments of inertia $\bar{I}$ and $\bar{J}$.

VI. Results and Discussion

Results obtained for the properties of equisided and elongated tetrakaidecahedron unit cells are shown in Tables 9 and 10, respectively. The results for E and ν match very well with the available analytical models: Zhu et al. [14] for an equisided tetrakaidecahedron unit cell and Sullivan et al. [13,17] for the elongated tetrakaidecahedron unit cell. The maximum error in the elastic constants was only 0.55% for the elastic moduli and 0.35% for the shear moduli in the case of the equisided tetrakaidecahedron unit cell. The maximum error in the elastic constants was 0.82% in the case of the elongated tetrakaidecahedron unit cell.

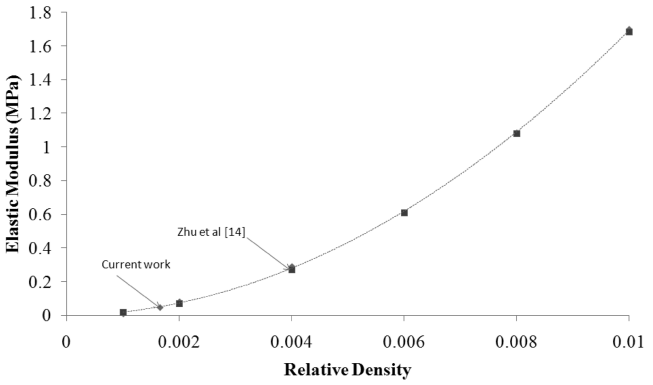

Fig. 13 Variation of elastic modulus with relative density for an equisided tetrakaidecahedron unit cell (curve-fit equation: $E_z = 16,545(\rho/\rho_s)^2 + 4.411(\rho/\rho_s) - 0.0034$).

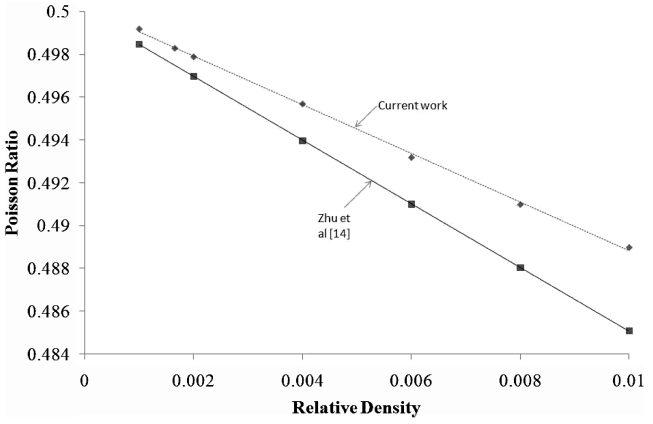

Fig. 14 Variation of Poisson ratio with relative density for an equisided tetrakaidecahedron unit cell.

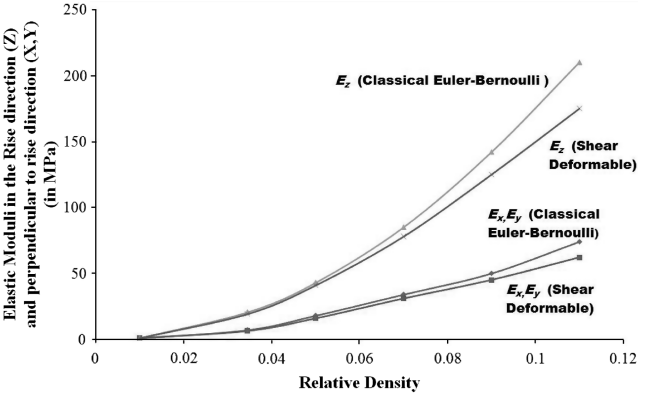

Fig. 15 Variation of elastic moduli in the rise direction (E_z) and perpendicular to the rise direction (E_x and E_y) with relative density for an equisided tetrakaidecahedron unit cell.

The deformed and undeformed configurations of the unit cell for various macrostrains are shown in Figs. 12a and 12b. In addition, results from parametric studies are shown in Fig. 15 for elongated foam.

It is interesting to note that with the equisided tetrakaidecahedron as the unit cell, the results for the properties using either Euler–Bernoulli or shear-deformable (Timoshenko) beam elements do not differ much (0.24% difference). This is because of the assumed beam aspect ratio ($L/d = 17$; see Fig. 3 and Table 1). With the beams being slender, the classical beam theory assumption holds well and the shear deformation is negligible. Hence, the Euler–Bernoulli and the Timoshenko beams give comparable results.

However, in the case of the elongated tetrakaidecahedron wherein the beams are short and thick, especially on the squares on the top and the bottom faces (Fig. 5, Table 2), the values for the properties have significant difference when a shear-deformable element is assumed instead of a Euler–Bernoulli beam element. The elastic modulus assuming shear-deformable beams is 9% lesser than the elastic modulus assuming Euler–Bernoulli beams, as shown in Table 10.

Figures 13 and 14 show the variation of elastic modulus and Poisson ratio with relative density. It is seen that the elastic modulus varies as square of the relative density. Figure 15 shows the variation of the elastic moduli in the rise direction and perpendicular to rise direction with relative density for the elongated tetrakaidecahedron unit cell. It is seen that as the relative density increases, the difference between the properties obtained from using Euler–Bernoulli elements and Timoshenko elements keeps increasing. Hence, the existing analytical models [13,14,17] assuming the unit-cell edges completely made out of Euler–Bernoulli beams would not be accurate, and bringing in the effect of shear deformation in the analytical formulation would be important.

The results of elastic constants for the variable-cross-section foam along with that of idealized uniform-cross-section foam are presented in Table 11. The relative density is assumed to be 0.165% in both

Table 11 Results compared for the properties of an equisided tetrakaidecahedron unit cell with relative density 0.1653% with uniform cross section and varying cross section

	Uniform cross section	Varying cross section	Ratio
Elastic modulus E, Pa	46,402	19,172	2.42
Shear modulus G, Pa	14,920	6183	2.41
Moment of inertia I, m^4	2.34×10^{-19}	0.965×10^{-19}	2.42
Poisson ratio ν	0.4975	0.4989	1.00

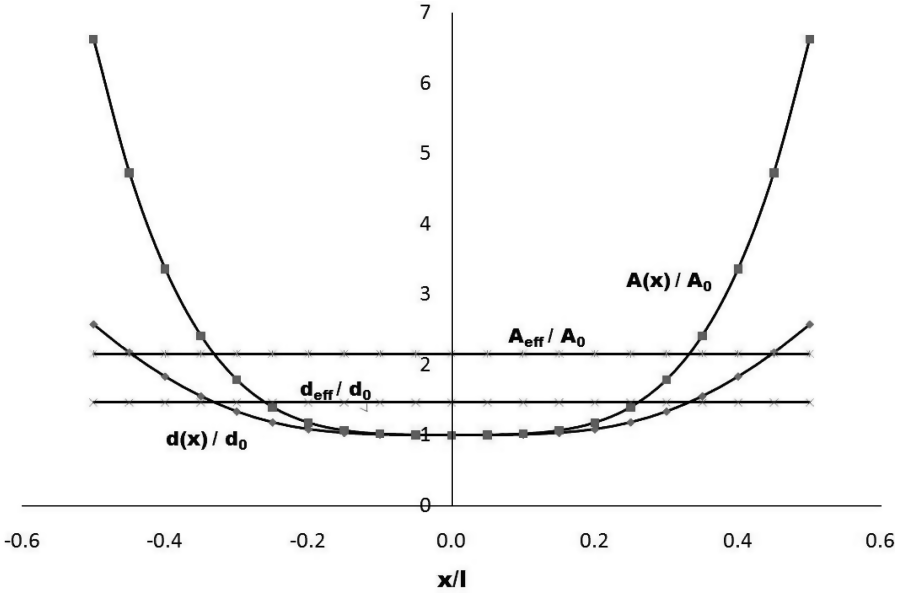

Fig. 16 Variation of area of cross section and the diameter of the cross section along the length of the strut.

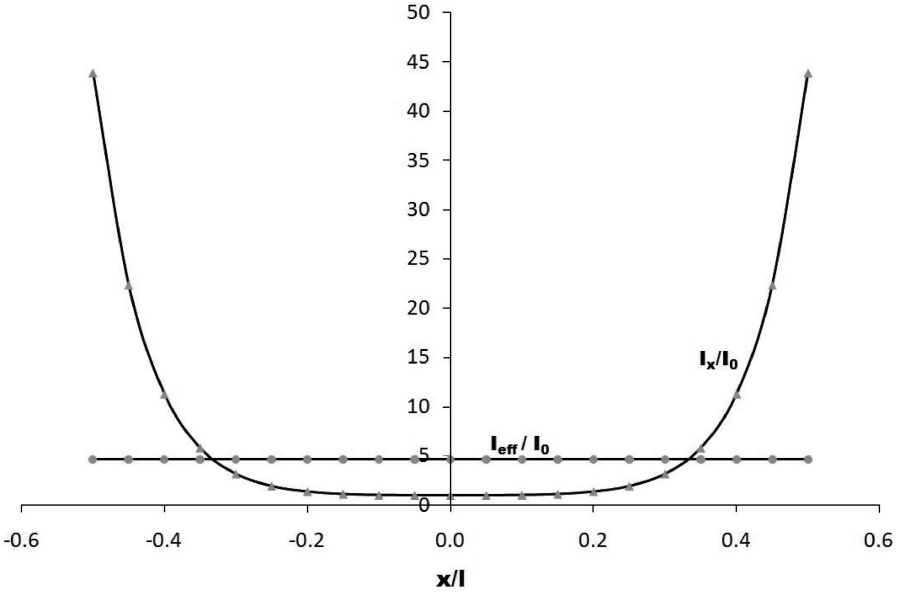

Fig. 17 Variation of moment of inertia along the length of the strut.

cases. It is seen that Young's modulus and shear modulus of ideal foams with uniform cross section is about 2.4 times that of varying-cross-section foam. The reason for this is that most of the solid material is near the ends (Figs. 16 and 17) of the strut, thus making majority of length (about 60%) in the middle slender. This reduces the moments of inertia considerably, making the struts more flexible. The variation of the moment of inertia, area of cross section, and diameter across the length of the strut are compared with those of uniform-cross-section foam in Figs. 16 and 17, respectively. Note that our analysis is restricted to foams that have a relative density below 0.2%, wherein the classical beam theory assumptions are valid. For higher relative densities, one should model the struts using three-dimensional solid elements to obtain accurate results, e.g., Gong et al. [16].

VII. Conclusions

Finite-element-based micromechanics have been used to calculate the elastic properties of foams with tetrakaidecahedral unit cells. The results for elastic constants match well with the available analytical models. It is evident that using finite element methods gives a flexibility to choose between Euler–Bernoulli formulation or the shear-deformable formulation or a mix of both in the same unit cell over the existing analytical models. The biggest advantage of using finite element methods is that any kind of a unit cell with unequal sides that might be obtained from microstructural measurements could be modeled with ease and the technique for computing properties would still remain the same. It would also be easy to extend the same finite element methods to calculate inelastic behavior of the foam. The same finite-element-based micromechanics methods could also be easily used in the unit-cell model to generate multi-axial failure envelopes for foams. The effect of varying cross sections on the elastic properties has been studied, and it has been shown that for the same relative density, foams with varying cross sections are less stiff compared with foams with uniform cross sections.

Note that in the current micromechanics-based approach, the assumption is that the foam is made out of exactly identical unit cells.

However, in reality, as seen in the micrographs in Fig. 1, the cell sizes can vary considerably and there are many discontinuities in the real material. One way of obtaining an estimate of properties of foam with varying cell sizes is as follows. The finite-element-based micromechanics approach presented here could be used to perform a sensitivity analysis of the elastic constants due to variation in parameters such as geometry and strut properties and then an appropriate averaging scheme could be used to determine the averaged properties.

Appendix: Analytical Expressions for Foam Elastic Constants

Summary of equations from Zhu et al. [14]:
Young's modulus E_{100}:

$$\frac{1}{E_{100}} = \frac{1}{6\sqrt{2}}\left(\frac{12L^2}{EA} + \frac{L^4}{EI}\right) \tag{A1}$$

Poisson ratio ν_{12}:

$$\nu_{12} = 0.5\left(\frac{AL^2 - 12I}{AL^2 + 12I}\right) \tag{A2}$$

Shear modulus G_{12}:

$$\frac{1}{G_{12}} = \frac{2\sqrt{2}L^2}{EA} + \frac{2\sqrt{2}L^4}{6EI}\left(\frac{8EI + GJ}{5EI + GJ}\right) \tag{A3}$$

Summary of equations from Sullivan et al. [13]:
Young's moduli (E_x, E_y):

$$E_x = E_y = \frac{12EI}{L\sin\theta[2L^3\sin^2\theta + b^3 + (12I/A)(2L\cos^2\theta + b)]} \tag{A4}$$

Young's modulus E_z:

$$E_z = \frac{24EI\sin\theta}{L^2(\cos^2\theta + (12I/AL^2)\sin^2\theta)(\sqrt{2}L\cos\theta + b)^2} \tag{A5}$$

Poisson ratios:

$$\nu_{xy} = \nu_{yx} = \frac{b(Ab^2 - 12I)}{12I(2L\cos^2\theta + b) + A(2L^3\sin^2\theta + b^3)} \tag{A6}$$

$$\nu_{xz} = \nu_{yz} = \frac{(AL^2 - 12I)(2L\cos\theta + \sqrt{2}b)\cos\theta}{2[12I(2L\cos^2\theta + b) + A(2L^3\sin^2\theta + b^3)]} \tag{A7}$$

$$\nu_{zx} = \nu_{zy} = \frac{\sqrt{2}L(AL^2 - 12I)\cos\theta\sin^2\theta}{(12I\sin^2\theta + AL^2\cos^2\theta)(\sqrt{2}L\cos\theta + b)} \tag{A8}$$

Summary of equations from Sullivan et al. [17]:
Shear modulus G_{xy}:

$$1\Big/\left(4l\sin\theta\left\{\frac{b}{EA} + \frac{l^3[(2 + 4\frac{b}{l}\cos^2\theta)EI + (\frac{b}{l}\sin^2\theta)GJ]}{12EI[(2 + \frac{b}{l}\cos^2\theta)EI + (\frac{b}{l}\sin^2\theta)GJ]}\right\}\right) \tag{A9}$$

Shear modulus G_{yz}:

$$1\Big/\left(\frac{l}{4\sin\theta}\left\{\frac{L[\frac{b}{l}\cos\theta + \sqrt{2}(1 + \sin^2\theta)]^2}{EA} + \frac{L^3[\lambda_1(EI)^2 + \lambda_2(EIGJ) + \lambda_3(GJ)^2]}{12EI[(1 + \sin^2\theta + 2\frac{b}{l}\sin^2\theta)(EI)^2 + (2 + 2\frac{b}{l}\cos^2\theta)EIGJ + (\cos^2\theta)(GJ)^2]}\right\}\right)$$

Please note that λ_1, λ_2, and λ_3 expressions have not been listed here and can be found in [17].

Acknowledgments

This research was supported by a State of Florida Space Research Initiative grant awarded to the University of Florida and University of Central Florida. The authors would also like to acknowledge support from the Florida Space Grants Consortium.

References

[1] Gibson, L. J., and Ashby, M. F., *Cellular Solids: Structure and Properties*, 1st ed., Cambridge Univ. Press, Cambridge, England, U.K., 1997.

[2] Thomson, W., "On the Division of Space with Minimum Partitional Area," *Philosophical Magazine*, Vol. 24, No. 151, 1887, p. 503.

[3] Hall, R. B., and Hager, J. W., "Performance Limits for Stiffness-Critical Graphitic Foam Structures, Comparisons with High-Modulus Foams, Refractory Alloys and Graphite-Epoxy Composites,". *Journal of Composite Materials*, Vol. 30, No. 17, 1996, 1922–1937.

[4] Li, K., Gao, X. L., and Roy, A. K., "Micromechanics Model for Three-Dimensional Open-Cell Foams Using a Tetrakaidecahedral Unit Cell and Castigliano's Second Theorem," *Composites Science and Technology*, Vol. 63, No. 12, 2003, pp. 1769–1781. doi:10.1016/S0266-3538(03)00117-9

[5] Arakere, N. K., Knudsen, E., Wells, D., McGill, P., and Swanson, G., "Determination of Mixed-Mode Stress Intensity Factors, Fracture Toughness, and Crack Turning Angle for Anisotropic Foam Material," *International Journal of Solids and Structures*, Vol. 45, Nos. 18–19, 2008, pp. 4936–4951. doi:10.1016/j.ijsolstr.2008.04.028

[6] Karkkainen, R., and Sankar, B. V., "A Direct Micromechanics Method for Analysis of Failure Initiation of Plain Weave Textile Composites," *Composites Science and Technology*, Vol. 66, No. 1, 2006, pp. 137–150. doi:10.1016/j.compscitech.2005.05.018

[7] Sankar, B. V., and Marrey, R. V., "Analytical Method for Micromechanics of Textile Composites," *Composites Science and Technology*, Vol. 57, No. 6, 1997, pp. 703–713. doi:10.1016/S0266-3538(97)00030-4

[8] Choi, S., and Sankar, B. V., "A Micromechanical Method to Predict the Fracture Toughness of Cellular Materials," *International Journal of Solids and Structures*, Vol. 42, Nos. 5–6, 2005, pp. 1797–1817. doi:10.1016/j.ijsolstr.2004.08.021

[9] Lee, S. J., Wang, J., and Sankar, B. V., "A Micromechanical Model for Predicting the Fracture Toughness of Functionally Graded Foams," *International Journal of Solids and Structures*, Vol. 44, Nos. 11–12, 2007, pp. 4053–4067. doi:10.1016/j.ijsolstr.2006.11.007

[10] Sullivan, R. M., Ghosn, L. J., and Lerch, B. J., "Application of an Elongated Kelvin Model to Space Shuttle Foams," *Journal of Spacecraft and Rockets*, Vol. 46, No. 2, 2009, pp. 411–418. doi:10.2514/1.37555

[11] Wright, L. S., and Lerch, B. A., "Characterization of Space Shuttle Insulative Materials," NASA TM-2005-213596, 2005.

[12] Huber, A. T., and Gibson, L. J., "Anisotropy of Foams," *Journal of Materials Science*, Vol. 23, No. 8, 1988, pp. 3031–3040. doi:10.1007/BF00547486

[13] Sullivan, R. M., Ghosn, L. J., and Lerch, B. J., "A General Tetrakaidecahedron Model for Open-Celled Foams," *International Journal of Solids and Structures*, Vol. 45, No. 6, 2008, pp. 1754–1765. doi:10.1016/j.ijsolstr.2007.10.028

[14] Zhu, H. X., Knott, J. F., and Mills, N. J., "Analysis of the Elastic Properties of Open-Cell Foams with Tetrakaidecahedral Cells," *Journal of the Mechanics and Physics of Solids*, Vol. 45, No. 3, 1997, pp. 319–343. doi:10.1016/S0022-5096(96)00090-7

[15] Weisstein, E. W., "Truncated Octahedron [online article]," *MathWorld*, Wolfram Research, Inc., Champaign, IL, http://mathworld.wolfram.com/TruncatedOctahedron.html [retrieved 2009].

[16] Gong, L., Kyriakides, S., and Jang, W. Y., "Compressive Response of Open-Cell Foams. Part 1: Morphology and Elastic Properties," *International Journal of Solids and Structures*, Vol. 42, Nos. 5–6, 2005, pp. 1355–1379. doi:10.1016/j.ijsolstr.2004.07.023

[17] Sullivan, R. M., Ghosn, L. J., and Lerch, B. J., "Shear Moduli for Nonisotropic, Open-Cell Foams Using a General Elongated Kelvin Foam Model," *International Journal of Engineering Science*, Vol. 47, No. 10, 2009, pp. 990–1001. doi:10.1016/j.ijengsci.2009.05.005

F. Wei
Associate Editor